QUT Digital Repository:
http://eprints.qut.edu.au/

QUT

This is the accepted version of this article. Published as:

Thilakarathna, Herath Mudiyanselage Indika and Thambiratnam, David and Dhanasekar, Manicka and Perera, Nimal (2010) *Numerical simulation of axially loaded concrete columns under transverse impact and vulnerability assessment.* International Journal of Impact Engineering, 37(11). pp. 1100-1112.

Numerical simulation of axially loaded concrete columns under transverse impact and vulnerability assessment

H.M.I. Thilakarathna*, D.P. Thambiratnam, M. Dhanasekar, N. Perera

Faculty of Built Environment and Engineering, Queensland University of Technology, GPO Box 2434, 2 George Street, Brisbane, QLD 4001, Australia

Abstract

With a view to assessing the vulnerability of columns to low elevation vehicular impacts, a non-linear explicit numerical model has been developed and validated using existing experimental results. The numerical model accounts for the effects of strain rate and confinement of the reinforced concrete, which are fundamental to the successful prediction of the impact response. The sensitivity of the material model parameters used for the validation is also scrutinised and numerical tests are performed to examine their suitability to simulate the shear failure conditions. Conflicting views on the strain gradient effects are discussed and the validation process is extended to investigate the ability of the equations developed under concentric loading conditions to simulate flexural failure events. Experimental data on impact force time histories, mid span and residual deflections and support reactions have been verified against corresponding numerical results. A universal technique which can be applied to determine the vulnerability of the impacted columns against collisions with new generation vehicles under the most common impact modes is proposed. Additionally, the observed failure characteristics of the impacted columns are explained using extended outcomes. Based on the overall results, an analytical method is suggested to quantify the vulnerability of the columns.

Keywords: Concrete columns, Transverse impacts, Numerical simulation, Vehicle collisions

1 Introduction

Columns in underground car parks, overpass bridges and medium to low rise buildings located close to major roads and intersections are highly vulnerable to impact loads from moving vehicles. Catastrophic failure of the supporting structure as a result of the impact worsens the consequences and hence requires proper analysis techniques which can be used for routine column design as well as damage mitigation. This paper describes the outcomes of a numerical simulation of reinforced concrete columns under transverse impact loads, which is further extended to assess the vulnerability of columns to vehicle impacts.

* * Corresponding Author: Mob. +61431094492*
*   Email:herath.thilakarathna@student.qut.edu.au*

There are few experimental investigations conducted on laterally impacted columns that demonstrate the effects of strain rate and confinement, particularly under mid span hard impact conditions [1]. However, the hard impacts usually represent the possible upper bound of the typical vehicle impacts [2] and hence generate over conservative results due to the exaggerated strain rate effects. In contrast, the energy based vulnerability assessment techniques presented in the literature [2] limit their application to columns that are fail in flexure under mid span low velocity impacts where strain rate and inertia effects are not predominant. The typical low elevation vehicle impacts initiate flexural-shear failure, a condition which is substantially different to flexural failure events under mid span impacts. Thus, research on shear critical RC columns under low elevation impact remains unexplored. Furthermore, since the impact response of columns is associated with higher modes of vibrations and various other vehicle specific parameters, the analysis process becomes quite complex [3, 4]. Consequently, the impact reconstruction techniques based on the deformable body assumption [5, 6] are largely simplified while the rest of the methods are limited to simulate an impact between a specific vehicle and a column [7]. These methods may not be reliable to assess the vulnerability of columns against a general vehicle population or new generation vehicles. As a result, the use of numerical methods for the vulnerability predictions of RC columns is exceptionally limited. This is also reflected by the generic and limited design guidelines provided in the current codes of practices [8, 9] which do not provide adequate design information on impacted columns [7]. Additionally, different design codes specify significantly different magnitudes for the expected quasi-static impact loading, which indicates a lack of understanding of the dynamic behaviour of both the column and vehicle [8, 9]. Hence, there exists a pressing need for the development of some simplified but rational methods to quantify the impact effects.

To address these issues, comprehensive impact analysis is conducted by using the finite element program LS-DYNA [10], incorporating steel reinforcement, confinement effects and strain rate effects. Contact definition, hourglass control and axial load application are among the other major considerations in the analysis. A constitutive material model that simulates failure under a tri-axial state of stress is used for concrete. The effects of the strain gradient are also considered and columns made of Grade 50 concrete under pure axial loading are investigated in detail. A simplified method based on the impact pulse generated from full scale impact tests is used for the impact reconstructions and the effects of the various pulse parameters are investigated for 15 to 60km/h velocity impacts. The attractiveness of the proposed method is that the outcomes can be used as a basis to generate a database for determining the vulnerability of columns to impact from new generation vehicles under all collision

modes. From the analyses, it has also been found that the vehicle impacts can be categorised close to the quasi-static loading region in typical force-impulse diagrams. This allows appropriate numerical methods to be implemented to quantify the vulnerability of the impacts.

2 Experimental test set up

Experimental data from the column tests of Feyarabend [11] are used in the validation process. The square RC column was tested in a horizontal position as shown in Figure 1. Fixed support conditions were achieved at one end by stationary steel sections fixed at the ground, and the other end was attached to a 20t mass that could slide over horizontal low friction rails simulating a roller support. The axial load was applied through a system of prestressing wires located on either side of the column, and the impact was generated by dropping a 1.14t mass on to the column at its mid span. The testing procedure involved impact test on 300×300mm square column specimen made of 47MPa concrete. The properties of the test specimen are given in Table 1 and a detailed description of the experimental program can be found in Feyerabend [11].

Figure 1: The test set-up by Feyerabend [11]

Table 1: Characteristics of the Feyerabend's test specimens [11]

3 Numerical simulation of the physical testing

As the entire structure does not have enough time to respond to a rapid change of loading under impact conditions [7], it was assumed that the lateral movements of the restraining mass and the elongation of the prestressing cable system during the impact do not affect the impact behaviour of the column. Hence the prestressed cable was excluded and the axial load was applied as a ramped up surface pressure over the cross section. The small fluctuation of the axial load due to the impact was also neglected as the fluctuation is unlikely to alter the flexural or shear capacity of the column.

Figure 2: The simplified test set-up and the cross section of specimen

The experimental set-up of the impacted column was simplified as shown in Figure 2. Half of the column was modelled and appropriate boundary conditions were introduced to maintain the symmetric conditions. Both supports were restrained against rotation while allowing translation along the longitudinal direction only at one end to simulate partial restrained conditions at the ends. These boundary conditions represent, as closely as possible, the complex support conditions used in the experiment. The concrete column was modelled using 25mm eight node hexagonal 'constant stress'

solid elements with one point integration. A numerical convergence study has showed that further decrease in the mesh size had only a very little effect on the accuracy of the results, while dramatically increasing the duration of the analysis. Consequently 25mm long beam elements with 2×2 Gauss integration were used for both the vertical and lateral reinforcements. The vertical reinforcements were defined as truss elements and the links were defined as Hughes-Liu beam elements with cross sectional integration [12]. A 35mm cover was provided for the reinforcement. Eight noded hexagonal solid elements with one point integration were employed for the drop mass. No attempt was made to simulate the guide rail or restraint when the drop mass bounces back after the first impact. A nominal radius was maintained at the bottom of the mass to avoid stress concentration along the perimeter, and initial analyses were carried out by assigning rigid body conditions [10]. Movement caused by the gravitational acceleration was not considered in the analysis as the main impact pulse lasted for a maximum of 10ms.

As far as deformed reinforcement bars are concerned, the ultimate dynamic bond at failure was 70-100% higher than that under quasi-static loading conditions [13]. Also, steel deformation under the impact load was limited to a region only a few centimetres long beneath the point of the impact [14]. This means that there is not enough time to develop extensive bond slip along the length of the bar during an impact. Therefore perfect bond was assumed between the reinforcement and concrete. Under these circumstances, strain hardening characteristics of the longitudinal steel may not alter the numerical results significantly.

3.1 *Contact algorithm and prevention of initial penetration*

The experimental program described in Section 2 consisted of impacting bodies having different stiffness. Consequently initial penetration occurred at the contact interface in the numerical simulation, which led to unrealistic localised stresses and strains. In order to prevent such contact break down, similar mesh discretisation was used for the drop weight and the column including the AUTOMATIC_SURFACE_TO_SURFACE [10] contact option. This standard penalty based formulation consists of interface springs between all the contact surfaces which apply interface forces proportionate to the amount of penetration. In a typical discrete environment the nodes of the softer body (slave) will be penetrated by the harder body (master). The selection of the slave and master surface can however be arbitrary with this formulation, since there are two checks for possible penetration between slave and master surfaces and vice versa. Since the default stiffness option of the contact definition depends

on the material properties and the size of the element, it was inadequate to handle the initial penetration between different materials. The soft constrained-based approach (SOFT=1) was effective in this circumstance where contact stiffness calculations are based on stability considerations by taking into account the time step. This option was particularly useful to address the dissimilarities of the mesh orientation and stiffness of the two bodies. The contact nonlinearity was further stabilised by assigning a value of 30 for the Viscous Damping Coefficient. In addition, friction coefficients were introduced to simulate the frictional forces that were transmitted across the contact interface due to the nominal radius that was maintained at the bottom of the impacting mass. The friction coefficients were assumed to be dependent on the relative velocity of the column (concrete) and rigid body (steel) that were in contact and consequently the selected values for the static and dynamic friction coefficients were 0.6 and 0.5 respectively [15]. A detailed description of the contact definition and the process for detecting and eliminating penetration can be found in the LS-DYNA user manual [10].

4 **Validation of the finite element model**

4.1 *Material characteristics*

Impact loads generate a tri-axial state of stress in concrete columns. For instance, from a material point of view, spalling occurs at the contact interface as a result of tri-axial extension stress conditions. Subsequently, tri-axial compression stress conditions are generated in the core concrete, and uni-axial tensile stresses will be generated at the face opposite to the impacted surface, by scabbing of the concrete due to wave reflection at the boundaries. Therefore, a material model that can replicate the results of tri-axial tension tests, tri-axial compression tests, and uni-axial tensile tests must be used in the impact simulation process. Each of these tests will represent different damage modes. However, there is also a possibility of combined failure modes.

The LS-DYNA material library has several material models that can be used to simulate the impact behaviour of concrete [10]. The material model *Concrete_Damage_REL3* was used in this investigation for the concrete. The advantage of this model is that the unconfined compressive strength and density of concrete are the two parameters that are required in the calibration process. However, if the response significantly differs from the observed behaviour of the concrete then the accuracy of the material model can be improved by calibrating additional model parameters [16, 17]. In addition, the model uses the unconfined compressive and tensile test paths to implement the rate enhancement effects. This method enables enhancement of the strength equally along any stress path and hence the different failure stress states such as uniaxial, biaxial and triaxial tension, and uniaxial and biaxial compression

all remain unaffected. Moreover, the model uses three failure surfaces; namely an initial yield surface, a maximum failure surface and a residual surface with consideration of all the three stress invariants (I_1, J_2 and J_3) [17]. Hence it can effectively simulate the tri-axial state of stress conditions. However, the mesh dependency of the fracture toughness has to be corrected by a single element analysis to enable simulation of tensile and shear failure conditions.

4.2 *Elimination of mesh dependency of the fracture toughness*

In this material model, the stress-strain curve for a particular concrete grade is generated by interpolating between the three failure surfaces using a parameter called $\eta(\lambda)$. λ is a non decreasing parameter which permits obtaining each point on the stress-strain curve by changing the value of $\eta(\lambda)$ from 0 to 1 and then decaying back to zero to represent softening. The parameter λ is given by;

$$\lambda = \begin{cases} \int_0^{\bar{\varepsilon}_p} \dfrac{d\bar{\varepsilon}_p}{r_f\left[1 + p/r_f f_t\right]^{b_1}} & p \geq 0 \\[4mm] \int_0^{\bar{\varepsilon}_p} \dfrac{d\bar{\varepsilon}_p}{r_f\left[1 + p/r_f f_t\right]^{b_2}} & p < 0 \end{cases} \quad , \qquad \text{Eq : 1}$$

which allows calculation of the damage in compression ($p \geq 0$) and tension ($p < 0$) separately, taking into account the strain rate effects. Descriptive details can be found in Malvar et al. [17] including the definitions of the relevant notations. In order to regulate the damage accumulation beyond the tensile failure where the above procedure fails, a volumetric damage increment can be added when required. The incremental damage is given by;

$$\Delta\lambda = b_3 f_d k_d \left(\varepsilon_v - \varepsilon_{v,yield}\right)_, \qquad \text{Eq : 2}$$

where b_3 is a user defined scalar multiplier, k_d is an internal scalar multiplier, ε_v represents the volumetric strain and $\varepsilon_{v,yield}$ is the volumetric strain at yield. As the softening part of the unconfined uni-axial tension stress-strain curve is governed by the values of the two parameters b_2 and b_3, these parameters have to be adjusted to minimise the differences between the numerical and the experiment results [17]. In addition, the softening behaviour becomes mesh-dependent if it is not governed by a *localisation limiter* or *characteristic length*. Thus, the mesh dependency of the fracture energy has to be corrected by changing the parameters assigned for the tensile softening of the material. The mesh dependency can be eliminated by selecting the size of the finite element h, so that the ratio G_f/h is equal to the area under the stress-strain curve for the uniaxial unconfined tensile test, where G_f is the

fracture energy of the concrete. This procedure eliminates the mesh size dependency of the fracture toughness.

Figure 3: Single element under uni-axial tensile test

Figure 3 shows the stress-strain response of a single element (1×1×1mm) subjected to uni-axial tension test. According to the CPF-FIP model code, the fracture energy of Grade 47 concrete should be in the range of 100Nm/m^2 to 125Nm/m^2 [18]. Hence, the default value of b_2 (b_2=1.35) will overestimate the fracture toughness of 47MPa concrete. Therefore, the value of b_2 is adjusted until the area under the stress-strain curve becomes 120Nm/m^2. However, no specific guidelines are found in the CEB-FIP code related to the strain rate effects on fracture toughness. Therefore strain rate effects are exempted from the fracture toughness and the selected value is based on the static material characteristics similar to the one used by Unosson [12]. Similarly, parameter b_3 is determined from the hydrostatic tri-axial tensile test. The default value of b_3 (b_3=1.15) leads to desired results and hence was accepted without alteration. The effects of these parameters are crucial where tensile and shear failure characteristics are more predominant.

4.3 *Material properties of steel*

Longitudinal reinforcement and hoops were modelled as elastic perfectly-plastic materials by using the *Mat_Plastic_Kinematic* model which has the reputation of minimising the duration of the analysis and is available for Hughes-Liu beam elements and truss elements [10]. Kinematic hardening with strain rate effects was implemented for the reinforcement. Table 2 represents the material properties adopted for the main reinforcement. Strain rate was incorporated using the Cowper-Symonds model given in Equation 3.

$$\frac{\sigma'_d}{\sigma_s} = 1 + \left(\frac{\dot{\varepsilon}}{C}\right)^{1/P}, \qquad \qquad \text{Eq : 3}$$

where, σ'_d is the dynamic flow stress at a uni-axial plastic strain rate $\dot{\varepsilon}$, and σ_s is the associated static flow stress. C and P represent the material constants. The relevant values for steel can be found in Table 8.1 of [19]. Failure strain was not defined here as there was no evidence of steel rupture.

Table 2: Material properties used for the main reinforcement

As the falling weight of 1.14t did not experience excessive deformations, a rigid material model was used for the impacting mass. Rigid elements are bypassed in the element processing and no storage is

allocated for storing history variables. However the inertial properties of the materials are calculated from the geometry of the elements and hence realistic values for the density and the modulus of elasticity must be provided. In addition, when the rigid body interacts with the column, the contact interface parameters are determined by using the given Young's modules, E and Poisson's ratio, ρ values of the material [10]. The material characteristics used for the drop mass are given in Table 3. Displacement and rotational degrees of freedom were constraints for the rigid body about the global X and Y directions.

Table 3: Material properties used for the Rigid Body

4.4 *Load simulation for a dynamic system*

When imposing static loads in an explicit environment the ramp up loading would be the best solution to avoid stress fluctuation. The ramp up load must be increased from zero to its final value and the load curve should extend beyond the termination time for stability. In general, the ramp duration should be greater than the fundamental vibration period (0.004s) of the column. Furthermore, it was observed that the stability of the simulation depends on the wave speed and the superimposing effects of the reflected waves at the boundaries. The minimum fluctuation was observed when the ramp duration was around 0.02s, above which there was instability again. The lateral impact force was applied after the vertical load stabilised. The rigid body was accelerated from zero velocity to 3ms^{-1} at impact over a 10mm gap. A realistic value for the density is essential for the rigid body since conventional equations of motion are involved in the velocity generation.

4.5 *Hourglass energy and damping effects*

Elements with reduced integration are more robust in impact simulations because the strain terms evaluated at the integration point remain well conditioned at larger deformations. However the disadvantage is that some modes of deformation may cause hourglass problems leading to inaccurate results. The hourglass resisting force vector $f_{i\alpha}{}^{k}$ is given in Equation 4 and descriptive details of each parameter can be found in [20]. In brief, the parameter $\Gamma_{\alpha\kappa}$ depends on nodal velocity and $h_{i\alpha}$ depends on nodal coordinates respectively.

$$f_{i\alpha}{}^{k} = a_h h_{i\alpha} \Gamma_{\alpha k} \qquad \text{Eq : 4}$$

where
$$a_h = Q_{hg}\, \rho\, v_e{}^{2/3}\, \frac{c}{4}. \qquad \text{Eq : 5}$$

Here v_e is the element volume, ρ is the density, c is the material sound speed, and Q_{hg} is a user defined constant. When Q_{hg} is equal to 0.05, improved results have been observed. As this equation contains a component of the volume v_e, theoretically the hourglass error should reach zero with the mesh refinements. Moreover, the default setting of LS-DYNA which is given by Equation 4 is not orthogonal. Therefore the orthogonal approach, as described by Flanagan and Belytschko [21] is used in this simulation. As far as the damping effects are concerned, damping forces do not impose significant effects during impacts where the duration of the event is shorter than the fundamental natural period of the specimen [22, 23, 24]. However, when damping effects were introduced to the system based on the 'mass weighted damping' method, which is ideal for damped low frequencies and rigid body motion [20], the deflection of the column and impact force reduced slightly with negligible increment of the contact duration. Since the procedure does not significantly improve the post peak behaviour of the column the damping effects were excluded. Moreover, the application of a specific damping coefficient cannot be justified in a realistic situation where the supporting structure has many elements that are interconnected.

4.6 *Procedure for axial load application*

Axial load on the column can be applied as a uniform surface pressure over the concrete area or as a combination of loads on the steel and concrete areas separately by assuming uniform strain distribution. Researchers have used the first option based on the assumption that a perfect bond between the concrete and steel can generate a uniform strain condition [25]. However it is prudent to investigate the above options in detail and select the one that minimises the error due to the contact enforcement.

In order to achieve the uniform strain condition a column subjected to pure axial compression must fulfil the following requirement.

$$\varepsilon_c = \varepsilon_s \qquad \text{Eq: 6}$$

where ε_c and the ε_s represent the longitudinal strain in concrete and steel respectively. For linear elastic behaviour, stresses in concrete and steel are in proportion to the modular ratio, $n = E_s / E_c$. Then, by considering axial load compatibility, it is possible to derive the following equation.

$$\sigma_c = \frac{N}{A_c} \frac{1}{1 + n\rho_{total}} \qquad \text{Eq: 7}$$

where N is the axial load on the column, A_c is the cross sectional area of the concrete column and ρ_{total} is the steel ratio of the section. This equation is based on the assumption that the strain of concrete and steel vary in an identical manner under the axial loads, which is not particularly true at the ultimate

stage. However the longitudinal steel yields before concrete. In addition, with the implementation of the axial load reduction factor $\phi=0.6$ according to AS 3600 [26] the error induced due to the assumption of strain compatibility can be neglected.

The lateral deflection of the column under the separate application of axial load on steel and concrete areas is different from that under a uniformly distributed load. This may cause a substantial difference of the failure load at near ultimate stage under lateral impacts and hence the full bond between concrete and steel will not ensure the strain compatibility, particularly close to the load application region. In fact, this would affect the shear capacity of the column under the lateral impact conditions. On the other hand, wave propagation effects through the material may alter due to the artificial stress concentration. Due to this same reason, applying the axial load separately enables acceptable performance as far as hourglass control is concerned. Consequently, the axial loads must be applied on steel and concrete areas separately and the numerical simulation process must contain a contact enforcement verification phase other than the mesh discretisation.

4.7 *Confinement effects under strain gradient*

The confinement effects can improve the strength and the deformability of the concrete columns under impact loading conditions while mitigating the damage. The confinement effects were therefore taken into account in the numerical simulation by assigning enhanced concrete characteristics to the core concrete and unconfined characteristics to the cover concrete based on the equations proposed by Mander et al. [27].

Figure 4: Lateral pressure distribution and the resultant strain gradient

It is worth investigating the capacity of this method to simulate concentrically as well as eccentrically loaded columns under impact. In fact, numerous models have been proposed to simulate the confined characteristics of concrete both under concentric [27, 28] and eccentric loading conditions [29, 30]. Enhanced stress-strain characteristics that develop under concentric loading conditions may not be applicable to eccentrically loaded conditions where the stress-strain distribution across the section substantially differs from that under concentric loading conditions (See Figure 4). Therefore the resultant strain gradient in eccentrically loaded columns was numerically simulated by dividing the cross section into a number of strips and then assigning various stress-strain characteristics based on the depth to the neutral axis [30]. The validity of such a method may be uncertain as impacted columns

may generate higher vibration modes where the compression and tension sides interchange over the height. However, in similar investigations, the confinement characteristics developed under concentric loading conditions were applied to eccentrically loaded columns [30, 31]. The results confirmed that the capacity predicted from the confinement characteristics developed under concentric loading conditions was adequate for evaluating the behaviour under eccentric loading conditions, particularly for low strength (56MPa or less) concrete columns. One of the assumptions of such investigation was that strength decay is essentially a function of confinement stress and does not vary with the strain gradient [29]. In addition, the investigation considered the fact that the stress-strain curves in the strips closer to the neutral axis may not be substantially different to the one that under fully confined conditions particularly in the preloading strain range [31]. Moreover, it is important to note that the flexural cracks appearing on the column at the ultimate stage under the impact will minimise the stress differences in various layers across the section. All these observations lead to the conclusion that vulnerability assessments of the eccentrically loaded columns are independent of confinement characteristics resulting from strain gradient. Therefore the present vulnerability assessment techniques could be extended to the eccentrically loaded columns by assigning uniform confined compressive characteristics to the core section.

4.8 *Comparison of numerical and experimental results*

Time histories of the mid span deflection of the impacted column as predicted by the FE model are compared with the published experimental data in Figure 5. The resultant maximum deflection and duration of the impact are well reflected in the results. Hence the inertia and stiffness of the impacting bodies, boundary conditions and effects of confinement are accurately simulated in the numerical model. Also, it is important to note that the residual displacement of the column was reasonably approximated by the numerical results even after cracking and slight crushing of the concrete during the impact as shown in Figure 6. Local crushing is important as this can reduce available energy and consequently modify the post impact behaviour of the impacted column. In addition the results confirmed the fact that the stress-strain characteristic developed under concentric loading conditions can be assumed over the entire core section to simulate the flexural failure conditions of impacted columns made of low grade concrete.

Figure 5: Comparison of the resultant deflections

Figure 6: Crack propagation of the impacted column and numerical simulation

The comparison of impact forces is shown in Figure 7 in which the continuous line represents the contact force history obtained through the numerical simulation and the dotted line represents the one that was obtained from the experimental test. It can be seen that the differences between the two graphs are insignificant and the impact-time histories are almost identical. On the other hand, the exact simulation of the peak contact force is evidence of the accurate representation of the stiffness and boundary conditions, as it would mainly depend on the inertia characteristics of the column for given boundary conditions. The comparison is quite good for both of these global parameters (impact force and deflection). Therefore the model as well as the input data used for the simulation can be regarded as satisfactory.

Figure: 7 Comparison of the resultant impact force

Figure: 8 Comparison of the resultant reaction force

Some differences are observed in the reaction forces generated by the numerical simulation compared to the experimental results (Figure 8). The sources of the error may be explained as follows. In the experiment, the load cells were placed in-between the bearing plates and the supports to measure the reaction. In the absence of descriptive details of the bearing system, the load cells were not modelled in the numerical simulation. However, the reaction forces are found to be very sensitive to the recording position [22]. Other possible reasons would be the inevitable error induced by the partial fixity of the supports due to the stationary steel sections, and the filtering procedure used to extract the data from the data logger system [11]. In spite of the differences in local peaks, the FE model prediction appears to be tracing the trend quite well.

The crack pattern predicted by the FE model of the impacted columns and that observed in the experiment were presented in Figure 6. Tension cracks initiated at the bottom and top of the beam followed by the crushing of the material beneath the impacted zone. The simulation reproduced the tension cracks at the bottom while displaying dense tensile crack propagation at the top surface of the beam. The dense crack concentration occurred directly beneath the impacted zone with the partial separation of the material represented as a region with higher stress accumulation. Based on these factors it can be concluded that the FE numerical simulation reasonably predicts the impact behaviour of the axially loaded column.

5 Impact reconstruction by using crash test data

The generation of realistic numerical models of vehicles for impact reconstruction is quite complex. On the other hand, specific methods used in the past are limited in their ability to asses the vulnerability of columns to impact from a general vehicle population [6, 7]. The crash response depends on the mode of impact, rate sensitivity of the vehicle, dynamic crush characteristics, restitution, collision partner and vehicle specific parameters [4]. Therefore the force time history of an impact at one particular velocity is different from vehicle to vehicle even though the mass remains the same. Consequently impact reconstruction with a rigid body or even with the simplified deformable body assumptions may not be adequate. It is therefore intended to reconstruct the vehicle impact by using various force pulses generated from full scale impact tests so that the generated results can be applied to a general vehicle population over the common modes of collisions.

5.1 *Vehicle column interaction*

The area of contact has some correlation with the mode of failure and the dissipation of kinetic energy through structural deformation. Hence, the vulnerability will depend on the distribution of the pressure over the contact interface. Eurocode EN 1991-1-7 (2006) suggests that the contact area should be 0.25m high for car impacts [9]. However, there is no guidance on the lateral distribution of the pressure across the section, particularly for circular columns. Figure 9 shows a rigid pole used to conduct several full scale impact tests on cars [32]. It is evident that the effective contact area is around 25% of the perimeter if the frictional effects are neglected. Therefore, a uniform normal pressure distribution is assumed across 25% of the perimeter and the resultant lateral pressure distribution used in this study is shown in Figure 10.

Figure 9: Front and side views of an impacted column [32]

Figure 10: Lateral pressure distribution across the diameter of the 300mm column

5.2 *Effects of the impact pulse parameters*

As impact pulse parameters play a vital role in the generation of a universal method to determine the vulnerability of columns under all collision modes, it is intended to investigate the effects of pulses generated from full scale vehicle to rigid barrier impacts in the impact reconstruction process. As observed in the literature, the triangular pulse shape is normally fitted with the force history diagrams generated from the frontal impact conditions [33, 34] while Sine, Haversine [35], and square formats

[36] are the other standard formats used widely to represent the frontal vehicle impacts. Numerical approaches to determine impact pulse parameters are rare in the literature as collision pulse characteristics depend on the mode of impact, collision partner and vehicle specific parameters. In fact, equations derived based on velocity profile, frontal stiffness, amount of deformation, and restitution may not be applicable to a general vehicle population [35].

Table 4: Comparison of the force time history data with properties of the impulse

Table 4 compares the area of the triangular impulse generated from the full scale impact tests [32], with the product of the mass and velocity of the respective vehicles. The force time history was obtained using the data generated by the accelerometer placed at the centre of gravity of the impacted vehicle. It is evident that the force pulse generated from the realistic impact events agree well with the product of the mass and velocity for the range of impact scenarios. This observation is effective in determining the basic pulse characteristic in the absence of precise numerical methods to quantify the collision pulses. Based on these results, the duration of the typical impact pulses can be assumed to be 100ms as they belong to a group of vehicles with various masses, stiffness and velocities. These force pulses will also be used for comparison purposes once the collapse load of the column is determined. In fact, force time history data generated from vehicle impact with rigid barriers are always conservative for the vulnerability assessment of deformable bodies such as concrete columns.

5.3 *Impact pulse modelling and pulse shape effects*

Figure 11: Iso-damage pulses

Figure 12: Effects of the strain rate or frontal stiffness

The effects of the pulse shapes are investigated in this subsection. Figure 11 shows the various pulses that lead to equivalent damage or iso-damage conditions. Triangular and Haversine failure amplitudes are almost equal, and the square pulse with equivalent ramp up duration is the one that causes the same damage with minimum peak. The observed impact behaviour is more sensitive to the peak impact force than the associated impulse similar to the quasi-static loading category where the response becomes insensitive to impulse [25]. It seems that the impact force is located close to the quasi-static region. The strain rate sensitivity of the impact can be examined by applying an equivalent peak force over a shorter duration (or by increasing the slope of the iso-damage functions) so that the strain rate accumulation in the column is enhanced. When the slope of the ramp function is increased, the column

fails at a lower amplitude (see Figure 12), even though the triangular force pulses implied the opposite [33]. In fact, inertia effects and the strain rate effects are the main parameters that govern the failure in this situation as the damping and deformation characteristics have negligible effects on energy dissipation during the impact. If the strain rate is the governing factor, the failure amplitude has to be increased due to the strength enhancement. However, as the column has failed at a lower amplitude, the inertia effects are more predominant than the strain rate effects for rectangular pulses in the quasi-static region (see Figure 12) and the opposite is true for triangular pulses. As the resultant variations are negligible, any of these characteristic curves for the vehicle impact generated force history space can be used to define a force-impulse diagram for the impacted columns when the structural damage is controlled by the shear capacity of the section. In this research only the triangular pulse is used to reconstruct the vehicle impact due to its simplicity. The peak force has been varied until the columns reach near ultimate stage while keeping the duration constant in order to account for the various masses and velocities. A comprehensive discussion on effects of impact duration will be provided at a later stage.

6 Simulation of impact of axially loaded columns in medium rise building

Impact capacity of typical columns of five to twenty storied buildings made of 50MPa concrete was investigated by using comprehensive numerical simulations. The columns support 6m spaning slabs in each direction, subject to $3kN/m^2$ imposed (live) load identical to the design load capacity of an office building, classrooms or lecture theatres at each floor level [26]. Vulnerability of a ground floor column was assessed for a typical frontal collision of light weight vehicles such as cars or vans. The structural design is based on the Australian Standard AS3600 [26]. However for comparison purposes the axial stresses on the columns are maintained approximately constant instead of the axial load on the columns. This has lead to smoother graphs at the later stage. In addition, two alternative design options with two different steel ratios were considered and Figure 13 represents the cross sections of the selected ground level columns supporting different number of stories.

Figure 13: Cross sectional areas of the circular concrete columns

Figure 14: Support conditions and external loads applications

Fixed support conditions were assumed in this analysis as the entire structure does not have enough time to respond [7]. Thus, translations as well as the rotations of all the nodal point in all directions are restrained at the bottom. The fixed end condition at the top is achieved by restraining lateral

movements of the circumferential nodal point in the global X and Y directions (Figure 14). The restrained height is maintained equal to the diameter of the column [37]. The free movement of the column along the vertical direction (Z) was allowed in order to permit axial shortening whilst allowing free vertical movements of the column during an impact.

Figure 15: Plan view of the half models

Quadratic solid elements were used at the core concrete zone (see Fig. 15) as the wedge element has caused stability problems under severe deformations including element interlocking. Obviously, the number of elements generated inside the rectangular segment (shown in Figure 15) is quite large and hence, stability of this model is high when it undergoes large deformations. These quadratic solid elements are the smallest elements in the entire model and the time step size has therefore been governed by the size of these elements.

6.1 *Impact behaviour of the columns and possible damage modes*

Once a triangular pulse is applied, the displacement of the column increases with the load until its peak is reached. Then the displacement decreases with several minor peaks in the post peak region until the residual displacement is achieved. This behaviour accounted for the axial load acting on the column, which has developed second order bending effects. In an actual impact event there could be some contact losses due to the relative movements of the bodies in this region as the speed of the deformation of the column exceeds the velocity of the vehicle even though they are moving in the same direction. According to further investigations a rapid change of residual deflection occurred with a small increment of the impact force at a later stage. Consequently the permanent damage to the column can be identified by the continuous increment of the residual deflection without recovering.

Failure due to vehicle impact, however, varies from the usual flexural type of failure under mid span impact and hence, a conventional hypothesis based on the energy absorption capacity of the column may not be applicable as the energy absorption characteristics mainly depend on the flexural deformation of the column. Since the column has not been subjected to flexural deformations, a small portion close to the impacted region has undergone highly localised stress and has absorbed an excessive amount of energy. This localised stress has exceeded the yield stress of the concrete and hence it may fail abruptly during the impact. This will considerably reduce the effective area of the column and the resultant eccentric axial load has finally diminished the axial load carrying capacity of

the column. Under these circumstances, the column has failed due to shear failure initially and subsequently by flexural failure leading to collapse. The observed failure modes can be categorised as shear or shear flexural type of failures depending on the test variables as observed during the many simulations.

Accordingly, the strain rate effects are more predominant in the vicinity of the impact and hence localised effects on the dynamic material characteristics could be significant. However the resultant overall capacity enhancement seems to be insignificant as the average strain rate was only marginal. For instance, the standard definition of the strain rate, $\dot{\varepsilon} = \dfrac{\delta \varepsilon}{\delta t}$ can also be expressed as $\dot{\varepsilon} = \dfrac{1}{L}\dfrac{\delta l}{\delta t} = \dfrac{v}{L}$,

where L is the original length of the element (column) and v is the rate of deformation. This definition generates a much broader view of the strain rate effects while allowing the average strain rate to be calculated. According to the Feyerabend column test [11], the maximum axial deformation of the column is around 1.3mm and the duration of the impact is approximately 6ms. This leads to an average strain rate of approximately $5.4 \times 10^{-5} s^{-1}$. As far as medium velocity vehicle impacts are concerned, the duration of the impact is around 100 ms and hence the average strain rate is well below $0.1 s^{-1}$.

6.2   *Vulnerability prediction*

The analyses include 300mm to 500mm diameter axially loaded columns which are adequate in capacity for five to ten story buildings with two different steel ratios as shown in Figure 13. The critical impact pulses for each column are given in Figure 16 along with the collision force-time histories of some cars - Honda Accord, Ford Taurus & Renault Fuego which are in frontal impacts similar to the one shown in Figure 17. Calculations based on the areas under the curves show that the axially loaded five-story building column design for gravity loads cannot withstand impact velocities more than 15ms^{-1} or 40 km/h (See Figure 16). This velocity range is common in urban areas and hence axially loaded column having diameters equal to or less than 340mm are likely to collapse under medium velocity car impacts. Though statement can not be generalised, this method will allow prediction of the vulnerability of the impacted columns against new generation of vehicles for most common modes of impacts and hence provide a common base for comparison purposes.

Figure 16: Comparison of impact capacities of columns with full scale crash tests

Figure 17: Honda Accord in a frontal collision at a speed of 48.3km/h [32]

If the impact duration remains constant, the peak force of the tri-angular pulse will determine the severity of the impact due to the negligible effects of the slope of its legs (see Figure 12). This observation implies that the peak forces can be interpolated to quantify severity of an impact. Based on this argument, it can be concluded that collision severity can be predicted by interpolating a known collision pulse as the influence of the slope of triangular pulse (or the strain rate effect) is negligible.

6.3 *Dynamic behaviour of the column due to impact*

Variation of the resultant bending moment due to impact was measured at three different locations along the height of the column in order to identify the impact behaviour of the column. The measured moments at each cross section (CS) are given in Figure 18 with the relevant distances measured from the bottom. The highest moments are generated in the vicinity of the impact (0.975m) and close to the support (0.100m), but with opposite signs. The moment gradually reduces away from the bottom support beyond the point of the impact. However another directional change can be seen close to the top support (3.9m) which signifies the generation of third order vibration mode in the impacted column. Consequently, excessive shear forces are generated at the contra-flexure points located close to the supports. This observation may be cited as a potential reason for the failure of the column shown in Figure 19 which indicates a typical shear critical situation. It is also important to note that laps forming in this region worsen the consequences. Thus, conventional design and detailing practices, which lead to impact damage, need modification. Laps should be avoided and transverse reinforcement should be provided close to the support where shear strength is vital for survival.

Figure 18: Resultant Bending moments for the 340mm column

Figure19: Damaged column under vehicle impact

6.4 *Effects of impact duration*

Figure 20 examines the impact characteristics of a 600mm diameter column with 4% steel. The column was subjected to equivalent impulses with different durations and the 100ms impact represents the critical pulse in which the column reached near failure conditions. In fact these impulses replicate the

cars with constant mass but with different frontal stiffness. Numerical results revealed that the column failed under 50ms impact while the column subjected to 150ms impact remains unaffected. This observation confirmed the importance of the frontal stiffness characteristics of the vehicle that govern the impact behaviour of columns. At the next stage, the peak forces of the triangular pulses are adjusted until the iso-damage (or equivalent damage) at near failure conditions are achieved as shown in Figure 21. Analyses under these pulse loads have shown that the column is highly sensitive to the amplitude of the impact pulse and not to the associated impulse. Thus, the vehicle impact generated forces are theoretically closer to the quasi-static loading category where the response becomes less sensitive to impulse [25].

Figure 20: Equivalent impulse diagrams   Figure 21: Iso-damage pulses for 600mm column

Another observation is that the impact pulses and resultant support reactions are nearly equal in terms of shape, duration and amplitude. According to Baker et al. [27], if the load and response functions terminate simultaneously, such a scenario can be included in the dynamic region which is between the impulsive and quasi-static regions. However, as the average strain rate was shown to be well below $0.1s^{-1}$ (in section 6.1), it can be concluded that the strain rate effects are less pronounced in the vehicle impact analysis.

Figure 22: Iso-damage contours for impact   Figure 23: A typical Pressure impulse curve

By considering all these factors, it is suggested that the vehicle impacts belong to a specific domain in the pressure impulse diagram. To investigate this hypothesis, force and the relative impulses that lead to the iso-damage conditions are plotted in a log scale for different column sizes (Figure 22). In fact, the curve reasonably agrees with the typical shape of the Pressure-Impulse diagram which is commonly adopted to predict the structural damage under blast loading conditions (Figure 23). Hence, the impact behaviour (in terms of amplitude *P,* impulse *I*) can be expressed by the following mathematical expression which is valid between the dynamic and the quasi static regions.

$$(P - P_o)(I - I_o) = A\left(\frac{P_o}{2} + \frac{I_o}{2}\right)^B \qquad \text{Eq: 8}$$

In the above equation, P_o and I_o represent a known force and impulse pair located on the iso-damage curve, *A* and *B* are constants to be determined based on the shape of the iso-damage contours. P_o and I_o can be expressed in terms of the column diameter, concrete grade, steel ratio, slenderness ratio and hoop spacing. A parametric study and the derivation of equations for the impacted column based on

this observation will be presented in a companion paper. Polynomial equations will be provided for more accurate estimations along with linear equations for approximate predictions.

7 Concluding remarks

This research has confirmed the feasibility of using numerical simulation techniques in vulnerability assessment of impacted columns while enhancing our understanding of the impact behaviour of columns under vehicular impacts. The main outcomes and findings of the investigations are summarised below.

1. Numerical model of an axially loaded column subjected to transverse impact loads has been validated and extended to simulate the behaviour of vehicle impacted columns. It is found that the numerical simulations of the column tests can be simplified greater by isolating the impacted column from the connecting structure and by assuming perfect bond between steel and concrete. However axial load must be applied separately on steel and concrete in order to maintain uniform strain distribution.

2. A material model that can replicate tri-axial state of stress must be used in the impact simulation process. LS_DYNA material model Mat_Concrete_Damage_REL3 fulfils the requirement. However the mesh dependency of the fracture toughness has to be corrected by a single element analysis to enable simulation of tensile and shear failure conditions. In addition, contact algorithms, hourglass problems and initial penetration condition must be treated carefully in the simulation process. Conversely, strain hardening and the strain rate effects of the longitudinal steel may not alter the result significantly. Damping effects may also be exempted from the numerical simulation.

3. For impact simulation, it is suggested that the application of the stress-strain models developed under concentric loading conditions is valid under eccentric loading conditions, particularly for lower grade of concrete.

4. Instead of simulating the impacted vehicle, impact pulse generated from a typical car to rigid barrier impact is successfully used to reconstruct the vehicle collision. This method can be used as the foundation to generate a data base which can be used to determine the vulnerability of column against most common modes of collision. Additionally, the rigid barrier-vehicle impact data are conservative in the impact reconstruction due to the low deformation of the column under shear predominant conditions.

5. If the duration and the peak force remain identical, the effects of the shape of the pulses are insignificant. Strain rate also has a negligible effect if the pulse characteristics belonging to the vehicle impact generated force history space. Inertia effects are more predominant than the strain rate effects for the rectangular pulses and the opposite is true for triangular pulses even though the comparative advantages are insignificant. Hence triangular pulses can be effectively used for impact simulations and the average duration can be taken as 100ms. In addition, collision severity can be predicted by interpolating known collision pulses as the strain rate effect is negligible.

6. The analysis also revealed that axially loaded five-story building columns are vulnerable to medium velocity car impacts. However at the design stage, impact capacity of the columns can be increased by 20% by selecting the alternative design method with the low amount of steel.

7. Resulting bending moments revealed the generation of third mode of vibration in the impacted column and generation of maximum shear forces at contra flexure points close to the supports. Consequently, the impacted column may tend to fail close to the supports under shear critical conditions. Thus, laps should be avoided close to the supports and maximum transverse reinforcement should be provided in the vulnerable regions to avoid shear failures.

8. The impacts of columns treated herein are theoretically close to the quasi-static loading region where the response becomes less sensitive to impulse, but more sensitive to the peak force. Iso-damage curves of the impacted columns will follow the shape of the conventional pressure impulse diagrams under blast loading conditions. Hence analytical equations can be derived to quantify the impact effects.

References

[1] Louw, M.J., G. Maritz, and M.J. Loedolff, The Behaviour of RC Columns under Impact Loading, The Civil Engineer in Sougth Africa, 1992: p. 371-378.
[2] Tsang, H. H., K. Rodsin, et al. (2005). "Collapse of reinforced concrete column by vehicle impact." 6th Asia-Pacific conference on Shock & Impact Loads on Structures, Perth, Australia.
[3] Hughes, G. and D.M. Speirs, An investigation of beam impact problems. Cement and Concrete Association, 1982. London.
[4] Varat, M. S. and S. E. Husher (2000). "Vehicle impact response analysis through the use of accelerometer data." SAE Technical Paper Series SAE World Congress, Detroit, Michigan.
[5] Campbell, K. L. (1974). "Energy Basis for collision severity" SAE Technical Paper.
[6] Prasad, A.K., Energy Dissipated in vehicle crush: a study using the repeated test technique, SAE Paper. Society of Automotive Engineers, 1990. Warrendale PA.

[7]   El Tawil, S., E. Severino, and P. Fonseca, Vehicle Collision with Bridge Piers. Journal of Bridge Engineering, 2005. 10(3): p. 345-353.

[8]   American Association of State Highway and Transportation Officials, Load and Resistance Factor Design AASHTO-LRFD. 1998. LRFD, bridge design specifications—Second edition, AASHTO, Washington, D.C.

[9]   EN 1991-1-7:2006, Eurocode 1 - Actions on structures - Part 1-7: General Actions & Accidental actions. Irish standards, 2006.

[10]   Hallquist, J.O. LS-DYNA 3D: User's manual, Livermore: Livermore Software Technological Corporation; V971, 2007.

[11]   Feyerabend, M., Hard transverse impacts on steel beams and reinforced concrete beams, PhD dissertation, University of Karlsruhe (T.H.),Germany, 1988.

[12]   Unosson, M., Modelling of concrete material behaviour with application to reinforced concrete beams subjected to impact, SE-147 25, 2001, Swedish defence research agency (FOI), Tumba. p. 33.

[13]   Weathersby, J.H., Investigation of bond slip between concrete and steel reinforcement under dynamic loading conditions. 2003, Louisiana State University and Agricultural & Mechanical College: United States-Louisiana.

[14]   Bentur, A., S. Mindess, and N. Banthia, The behaviour of concrete under impact loading: Experimental procedures and method of analysis. Materials and Structures, 1986. 19(5): p. 371-378.

[15]   McCormick, J., et al., Investigation of the sliding behaviour between steel and mortar for seismic applications in structures. Earthquake engineering and structural dynamics. 2009: John Wiley & Sons, Ltd.

[16]   Schwer, E.L. and L.J. Malvar, Simplified concrete modelling with Mat_Concrete_Damage_ REL3. JRI LS_DYNA user week, 2005.

[17]   Malvar, L.J., et al., A plasticity concrete material model for DYNA3D, International Journal of Impact Engineering, 1997. 19(9-10): p. 847-873.

[18]   CEB-FIP, CEB-FIP Model Code 1990, Redwood Books, Trowbridge, Wiltshire, UK, 1990.

[19]   Stouffer, D.C. and L.T. Dame, Inelastic Deformation of Metals: Models, Mechanical Properties, and Metallurgy. 1996: New York: John Wiley and Sons. 520 pages.

[20]   Hallquist, J.O. (2006). LS-DYNA 3D: Theoretical manual. Livermore, Livermore Software Technology Corporation.

[21]   Flanagan, D.P., Belytschko, T., A uniform strain hexahedron and quadrilateral with with orthogonal hourglass control. International Journal for Numerical Methods in Engineering, 1981. Vol. 17: p. pp.679-706.

[22]   Zeinoddini, M., J.E. Harding, and G.A.R. Parke, Axially pre-loaded steel tubes subjected to lateral impacts (a numerical simulation). International Journal of Impact Engineering, 2008. 35(11): p. 1267-1279.

[23]   Jones, N. Structural impact: Cambridge: Cambridge University Press, 1997. p. 333-385.

[24]   Strong, W.J. and T.X. Yu. , Dynamic Models for Structural Plasticity. 1993: Springer, London, UK: 1993. p. 112-155.

[25] Shi, Y., H. Hao, and Z.X. Li, Numerical derivation of pressure-impulse diagrams for prediction of RC column damage to blast loads, International Journal of Impact Engineering, 2008. 35(11): p. 1213-1227.

[26] AS 3600, Concrete structures, 2004: p. 185.

[27] Mander, J.B., M.J.N. Priestley, and R. Park, Theoretical stress-strain model for confined concrete. Journal of Structural Engineering, ASCE, 1988. 114(8).

[28] Sheikh, S.A. and S.M. Uzumeri, Analytical Model for Concrete Confinement in Tied Column. Journal of Structural Engineering, ASCE, 1982. 108(ST12): p. 2703-2722.

[29] Sargin, M., S.K. Ghosh, and V.K. Handa, Effects of lateral reinfocement upon the strength and deformation properties of concrete. Mag. Concrete Res., 1971. 28(75-76): p. 99-110.

[30] Lokuge, W.P., S. Setunge, and J.G. Sanjeyan, Modelling eccentrically loaded high-strength concrete columns. Magazine of Concrete Research, 2003,. 55(4): p. 331-341.

[31] Saatcioglu, M., A.H. Salamat, and S.R. Razvi, Confined columns under eccentric loading. Journal of Structural Engineering, ASCE, 1995. 121(11): p. 1547–1556.

[32] http://www-nrd.nhtsa.dot.gov/database/nrd-11/veh_db.html

[33] Thilakarathna H.M.I. et al., Behaviour of Axially Loaded concrete columns subjected to transverse impact loads, 34th conference on our world in concrete & structures, 2009, Vol XXVIII, p. 359-365.

[34] Breed, D.S., V. Castelli, and W.T. Sanders, A New Automobile Crash Sensor Tester. SAE Technical Paper 910655, 1991. Society of automotive engineers, Warrendale, PA.

[35] Varat, M.S. and S.E. Husher, Crash Pulse Modeling for Vehicle Safety Research, 18th ESV Paper, Paper 501, USA, 2000.

[36] Brach, R.M., Mechanical Impact Dynamics. 1991, New York: John Wiley and Sons Inc.

[37] BS 8110, Part 1: structural use of concrete. British Standards Institution, 1985. London. p. 118.

[38] Baker, W. E., P. A. Cox, et al. (1983). "Explosion hazards and evaluation." Amsterdam, New York; Elsevier Scientific Pub. Co.; 1983.
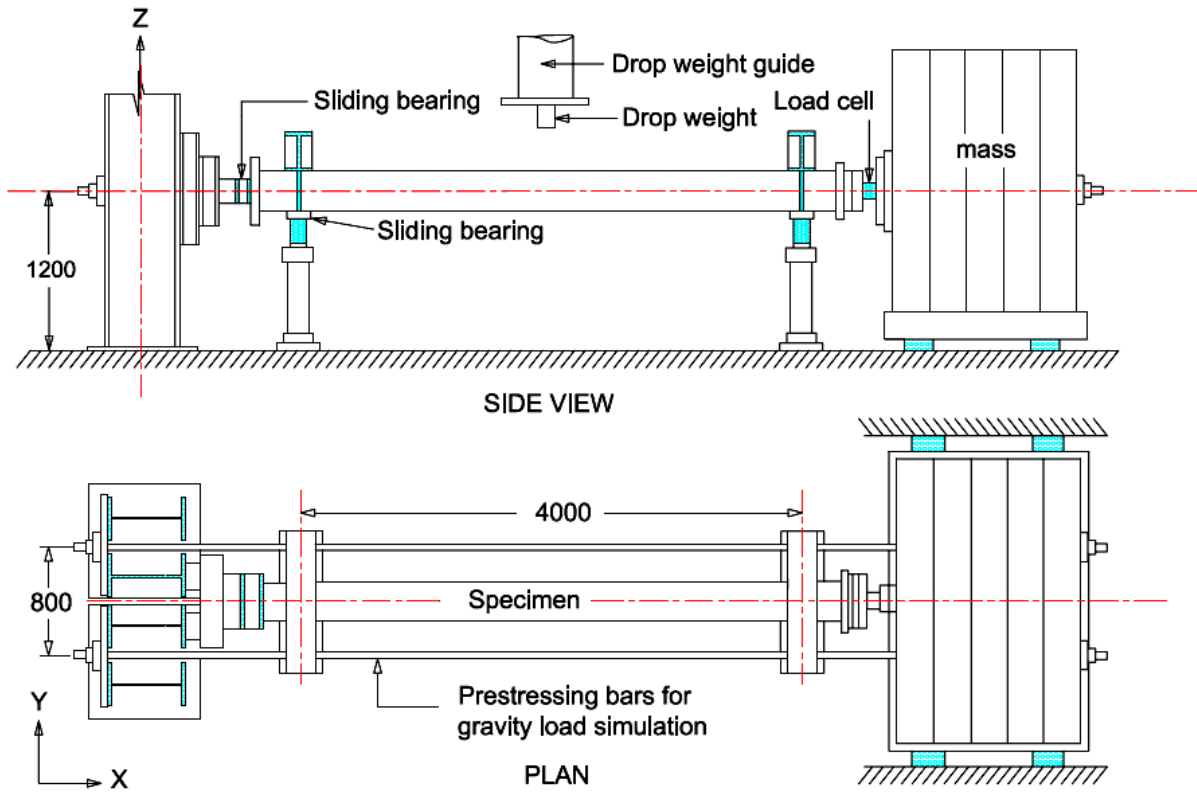
Figure 1: The test set-up by Feyerabend [11]
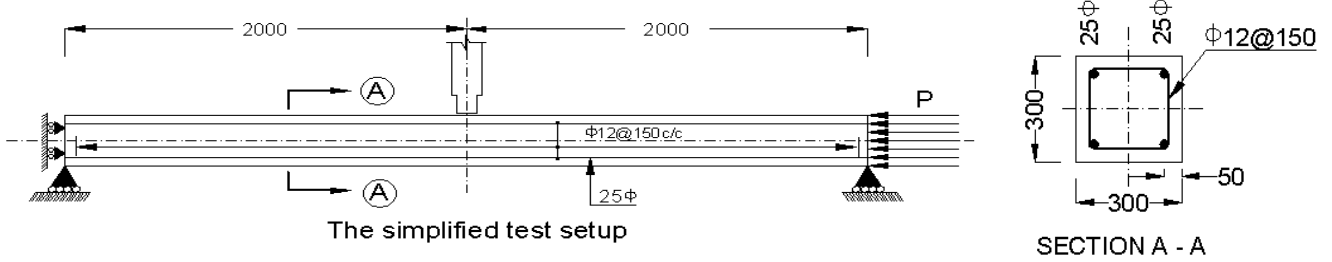
Figure 2: The simplified test set-up and the cross section of specimen
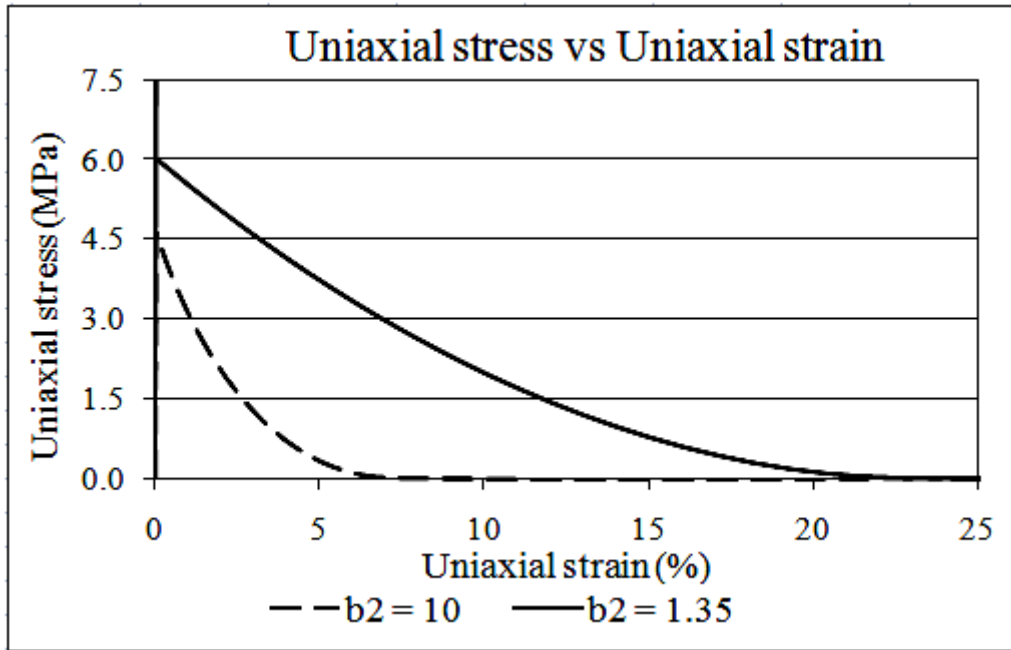
Figure 3: Single element under uni-axial tensile test
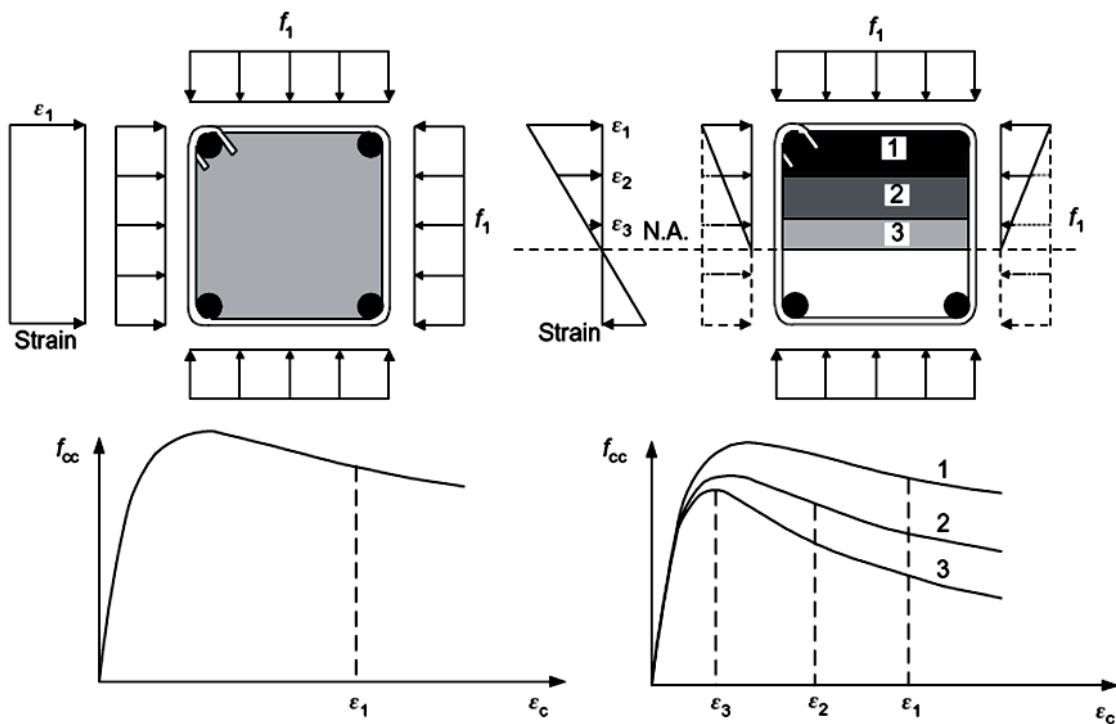
a) Section under concentric loading   b) Section under eccentric loading

Figure 4: Lateral pressure distribution and the resultant strain gradient
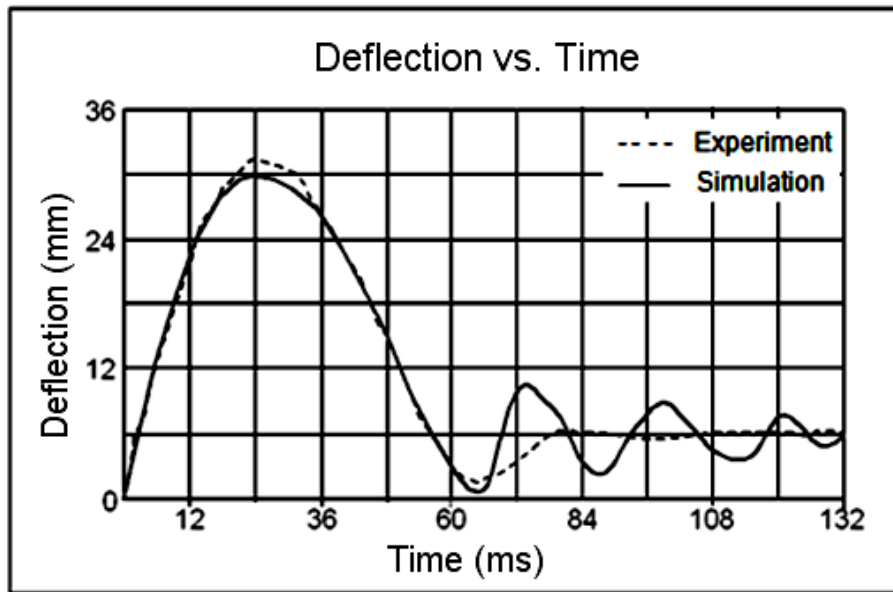
Figure 5: Comparison of the resultant deflection

SB2, $v_0 = 3.0ms^{-1}$
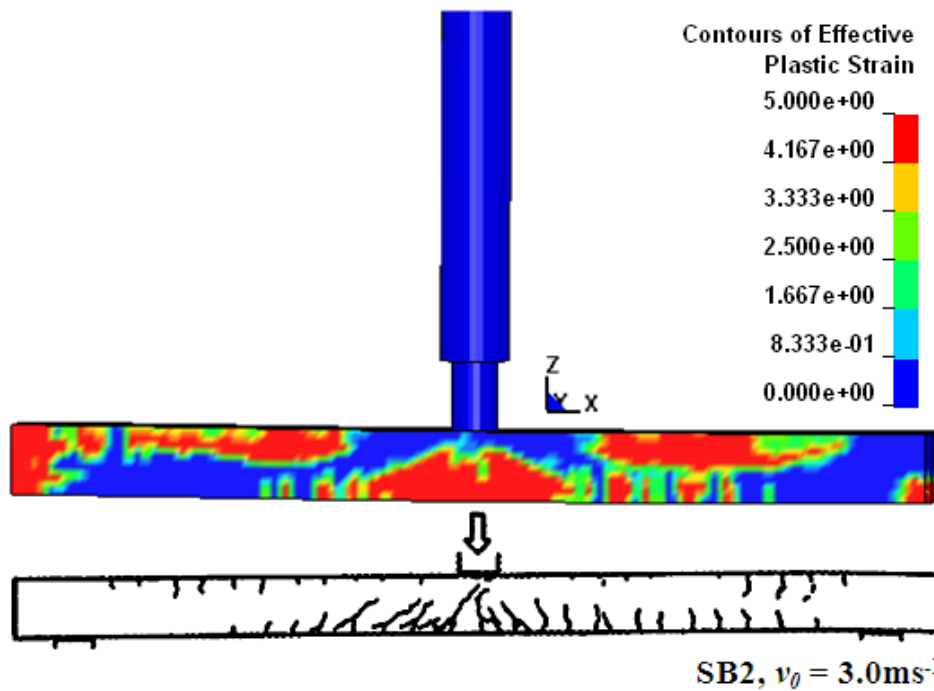
Figure 6: Crack Propagation of the impacted column and numerical simulation
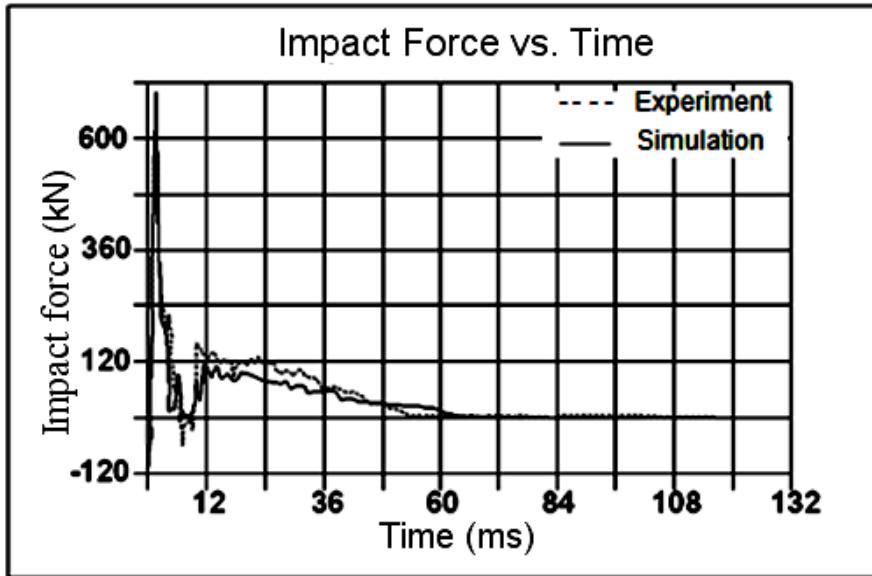
Figure: 7 Comparison of the resultant impact force
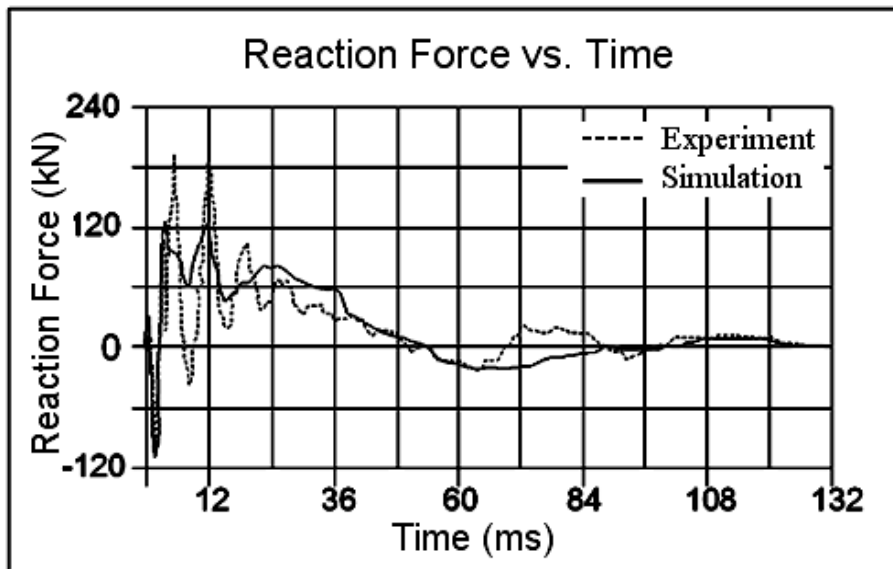
Figure: 8 Comparison of the resultant reaction force
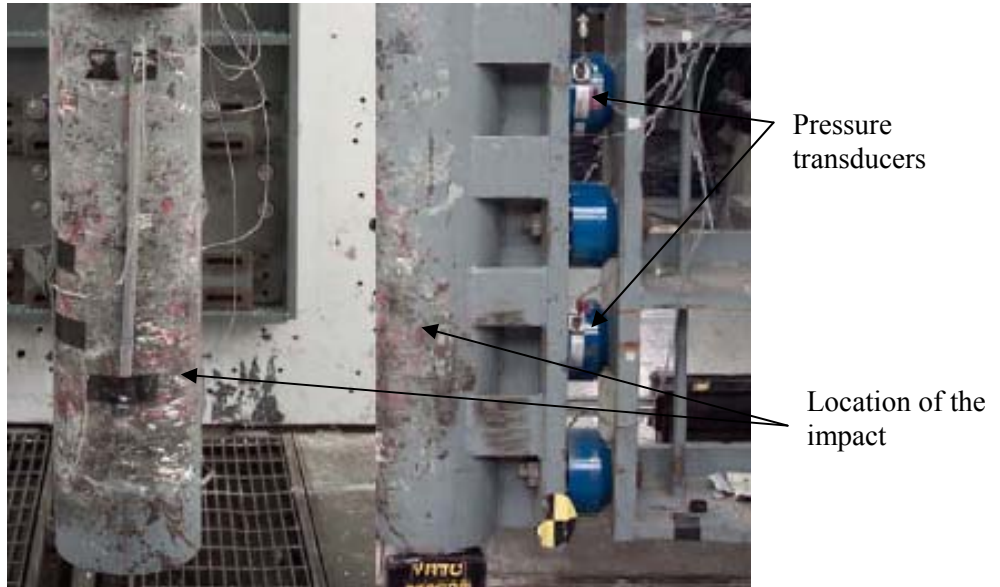
Figure 9: Front and side views of an impacted column [32]
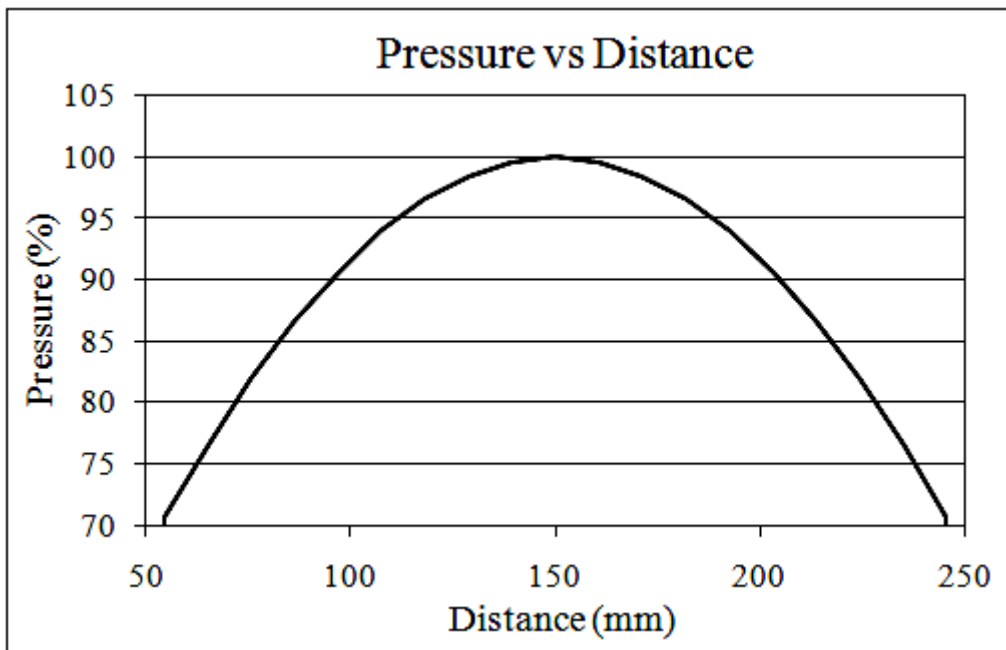
Figure 10: Lateral pressure distribution across the diameter of the 300mm column
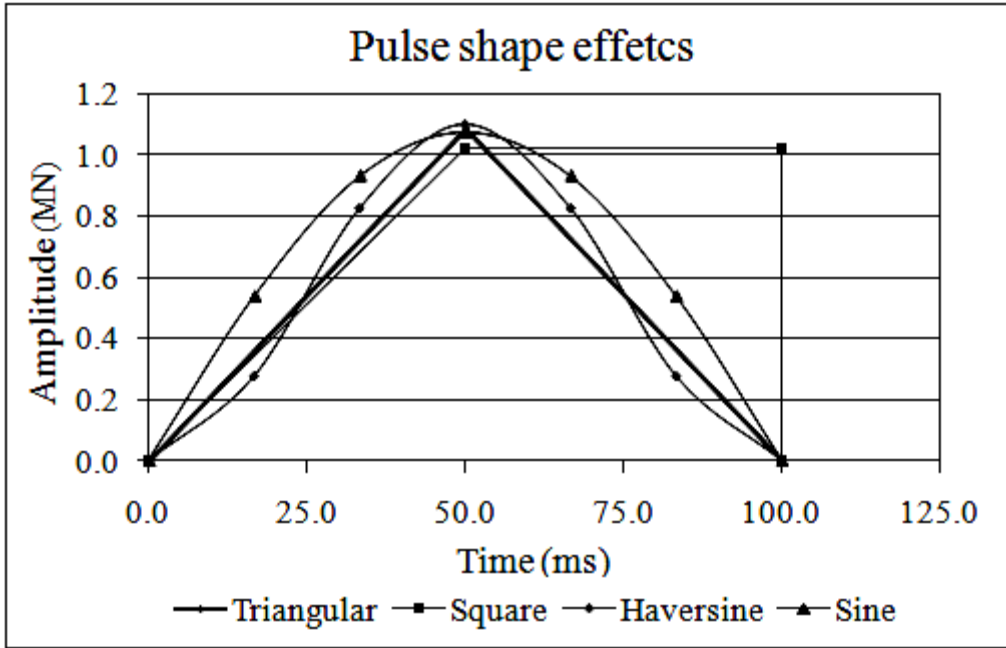
Figure 11: Iso-damage pulses
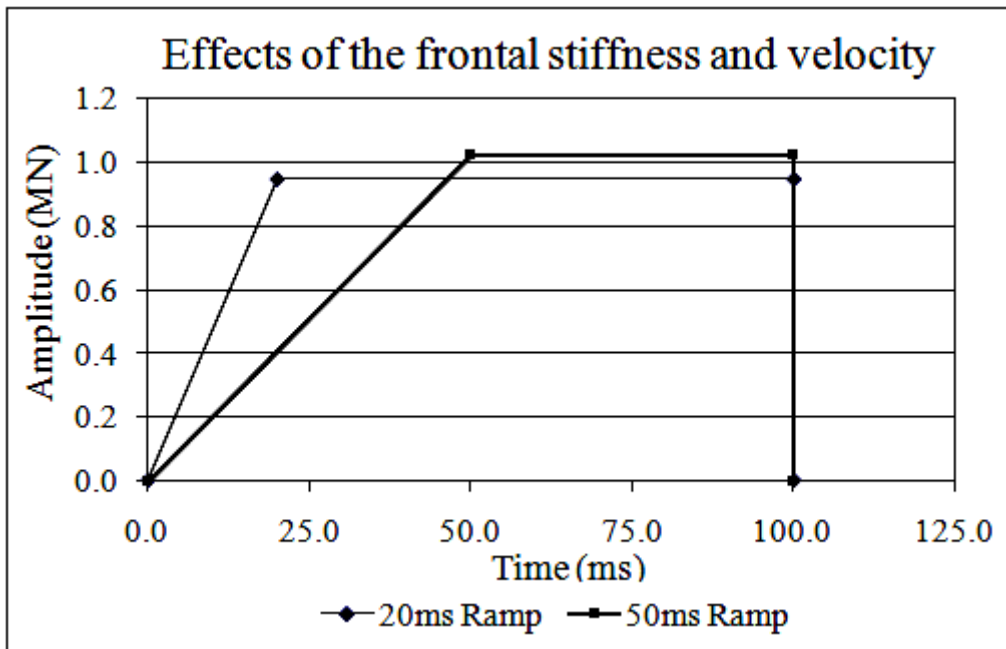
Figure 12: Effects of the strain rate or frontal stiffness
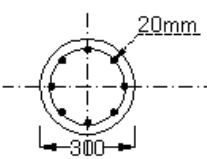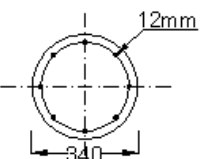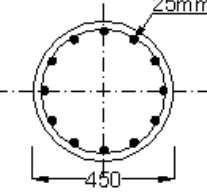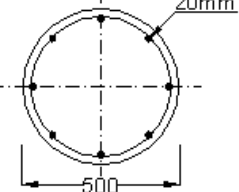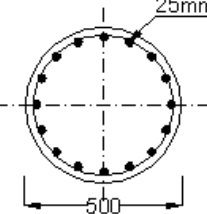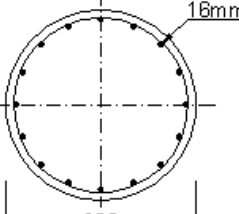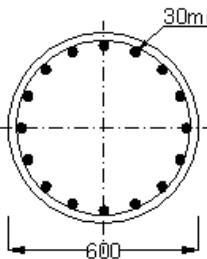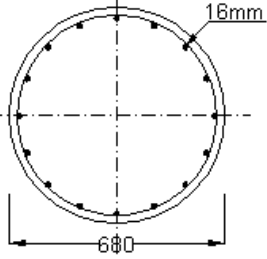
No. of Stories	Max. Steel (4%)	Min. Steel (1%)
5	20mm / 300	12mm / 340
10	25mm / 450	20mm / 500
15	25mm / 500	16mm / 600
20	30mm / 600	16mm / 680

Figure 13: Cross sectional areas of the circular concrete columns
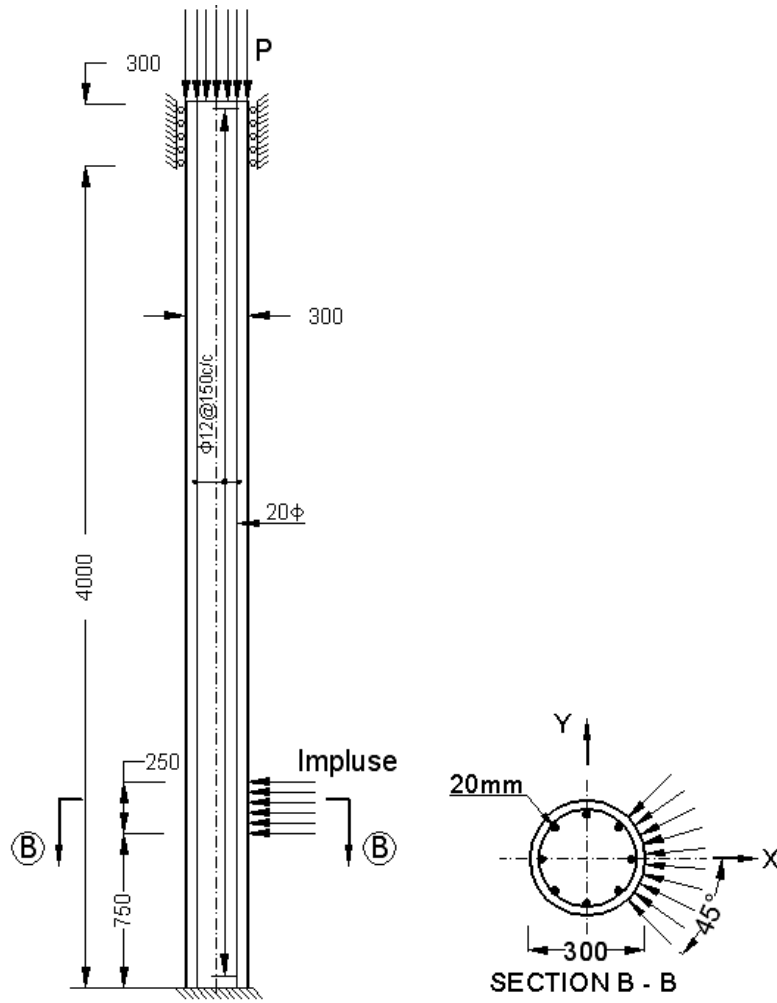
Figure 14: Support conditions and external loads applications
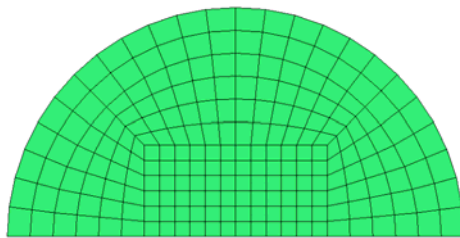
Figure 15: Plan view of the half models
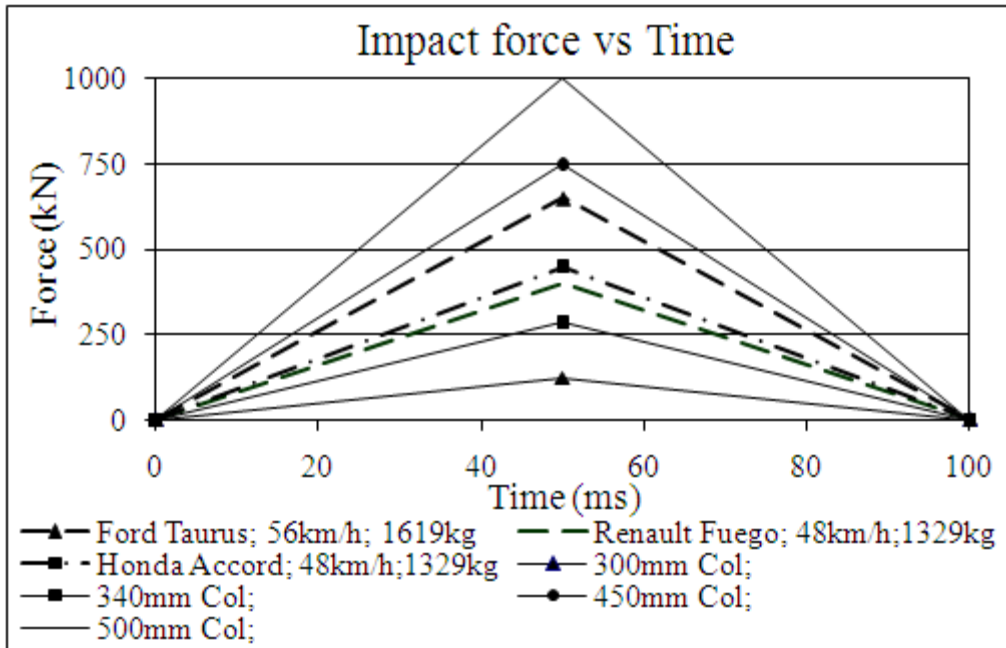
Figure 16: Comparison of impact capacities of columns with full scale crash tests
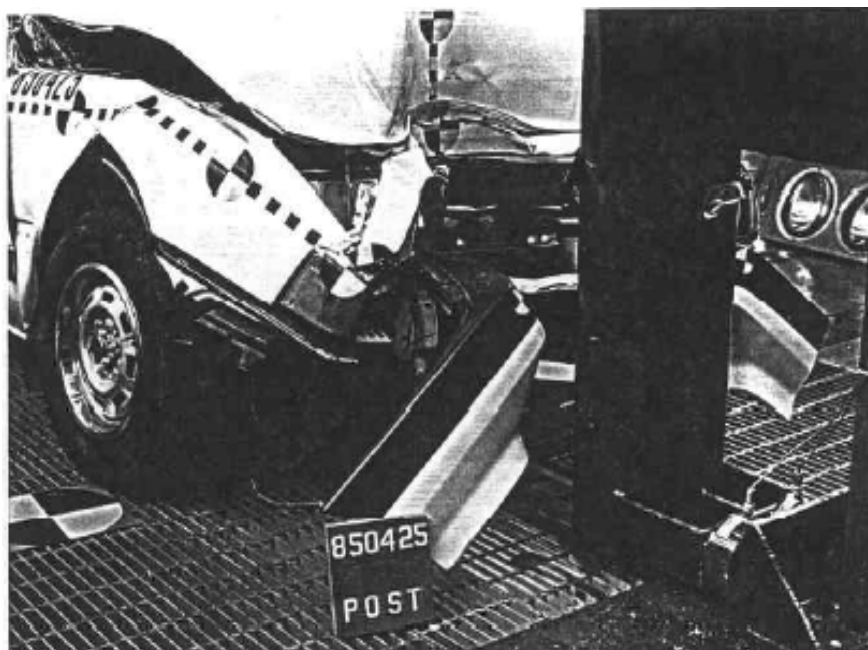
Figure 17: Honda Accord in a frontal collision at a speed of 48.3km/h [32]
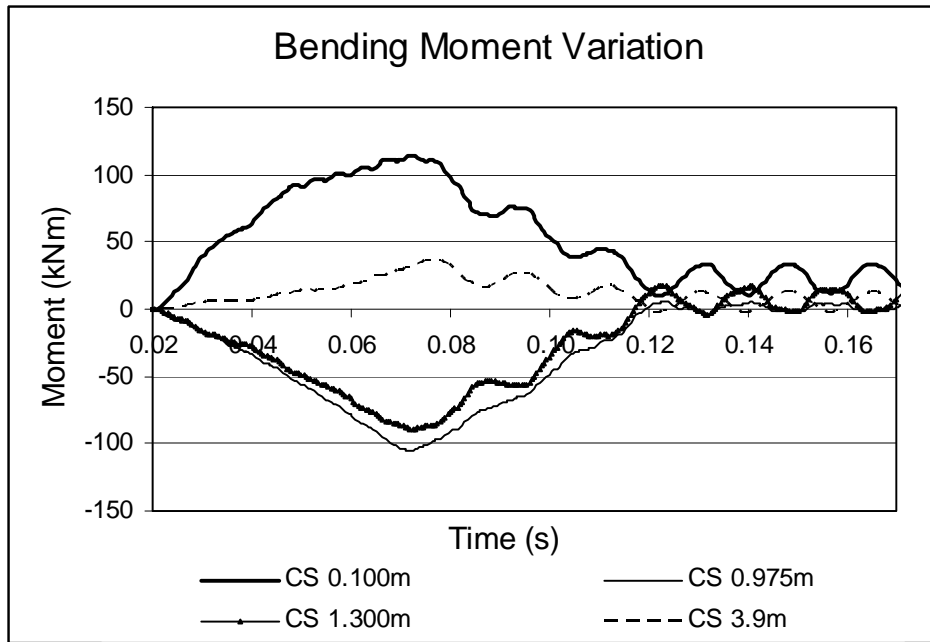
Figure 18: Resultant Bending moments for the 340mm column
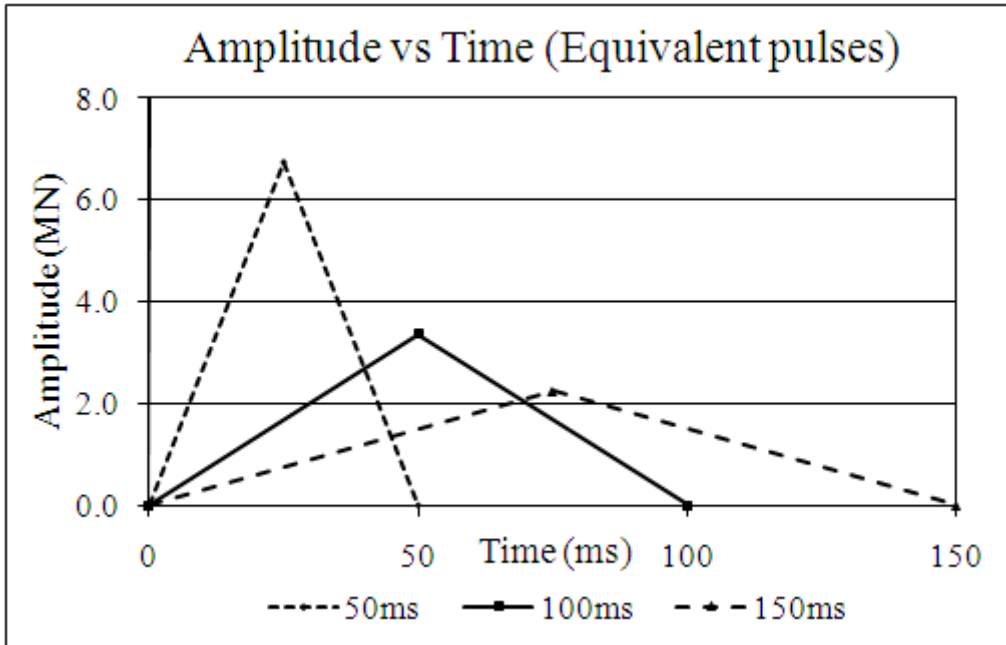

Figure19: Damaged column under vehicle impact
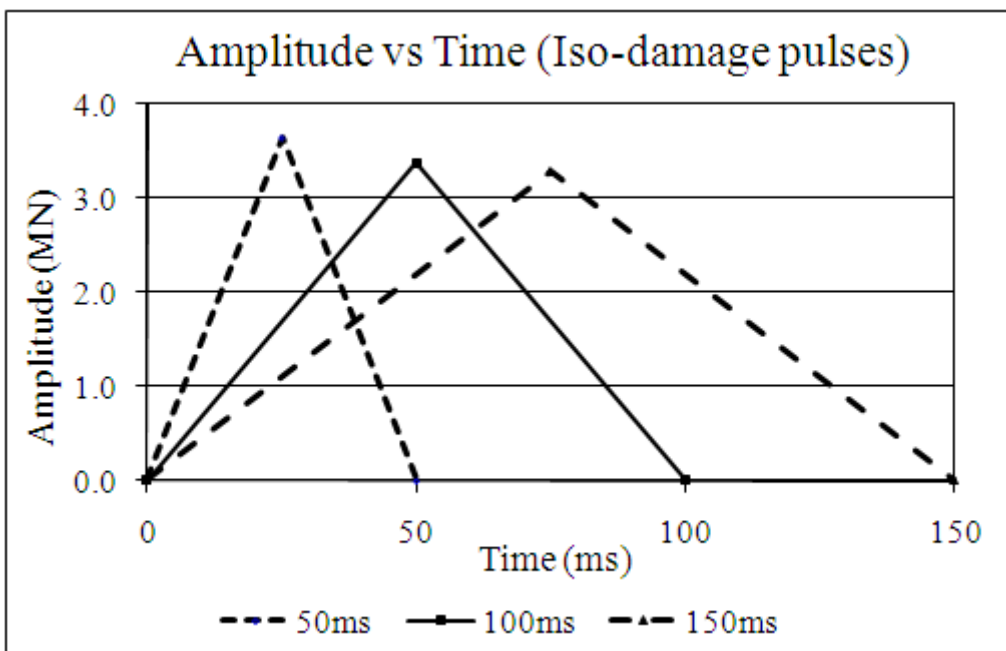
Figure 20: Equivalent impulse diagrams

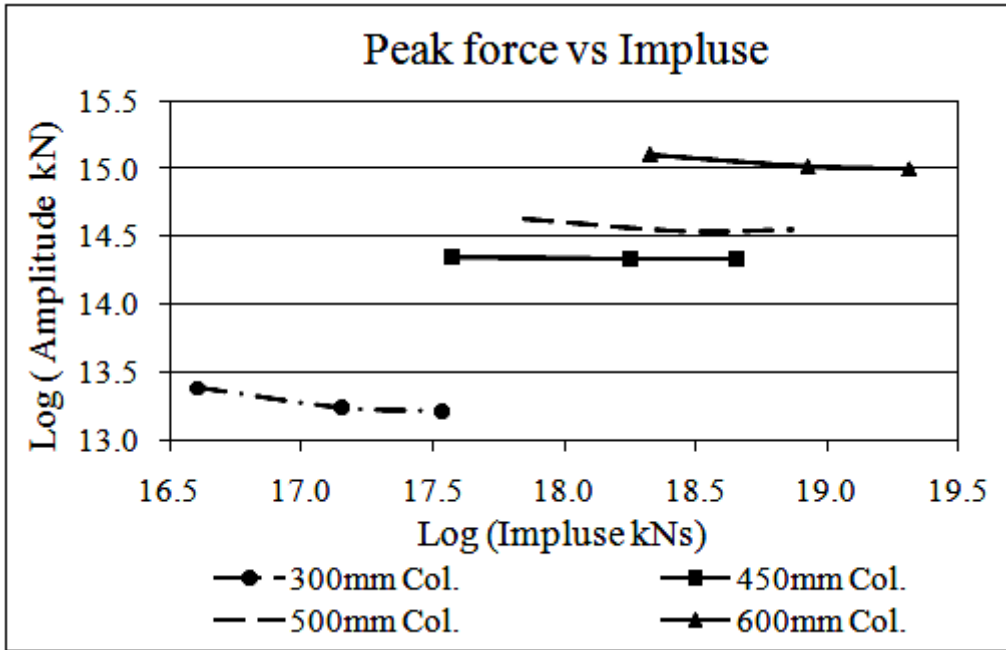Figure 21: Iso-damage pulses for 600mm column

Figure 22: Iso-damage contours for impact

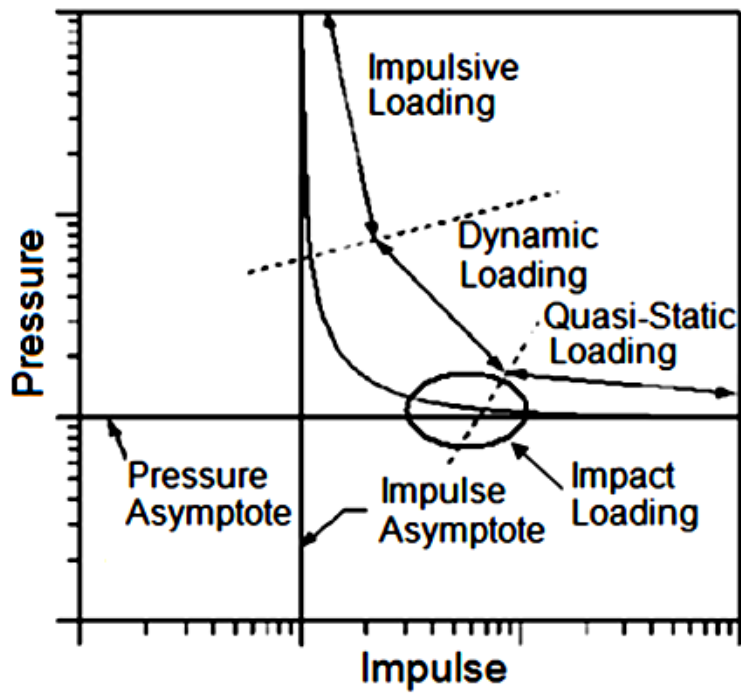Figure 23: A typical Pressure impulse curve

Details of test No.SB2	
Cross-section (m×m)	0.3×0.3
Span (m)	4.0
Concrete cube strength, f_{cu} (MPa)	47
Steel Yield stress, f_y (MPa)	548
Main bars, d_s (mm)	$4\phi25$
Shear stirrups, A_{vs} (mm/mm)	$12\phi@150$
Restraining mass (kN)	196.2
Initial axial load (kN)	-197
Striker mass (kN)	11.18
Impact velocity (m/s)	3.0
Velocity at which f_y was reached (m/s)	±1.8

Table 1: Characteristics of the Feyerabend's test specimen [11]

Density (kg/m^3)	E_s (GPa)	Poisson's ratio ρ	σ (MPa)	E_t (GPa)	Hardening Parameter (β)	C	p
7800	210	0.30	548	2.0	0	40	5

Table 2: Material properties used for the main reinforcement

Density (kg/m^3)	Young's Modulus (GPa)	Poisson's ratio
7800	210	0.3

Table 3: Material properties used for the Rigid Body

Vehicle	Velocity V(ms^{-1})	Mass M (kg)	Impact Duration (s)	(MV)	Area of the curve	Percentage variation
Ford Explorer	16.9	2242	0.150	37890	39573	1.04
Ford Taurus	15.6	1619	0.100	25274	27794	1.09
Renault Fuego	13.3	1329	0.100	17793	16687	0.94
Honda Accord	13.4	1329	0.100	17830	19500	1.09

Table 4: Comparison of the force time history data with properties of the Impulse